

Self-propelled dynamics of deformable domain in excitable reaction diffusion systems

Takao Ohta

Abstract.

The time-evolution equations for an isolated domain in an excitable reaction-diffusion system are derived both in two and three dimensions by an interfacial approach near the drift bifurcation where a motionless state becomes unstable and a domain starts propagation at a certain velocity. The coupling between shape deformation of domain and the migration velocity is taken into consideration. When the relaxation of shape deformation is slow enough, a straight motion becomes unstable and several kinds of motion of domain appear depending on the parameters. The self-propelled domain dynamics under the external fields is also studied.

§1. Introduction

Self-organized dynamics of domains in reaction-diffusion media have attracted much attention for more than two decades [1]. Computer simulations of reaction-diffusion equations have revealed various interesting dynamics of domains. For example, Krischer and Mikhailov have investigated numerically domain dynamics in two dimensions in an excitable reaction-diffusion system with a global coupling [2] and have found that a motionless localized domain loses its stability and begins to propagate when a system parameter exceeds a certain threshold. This is called a drift bifurcation. They have shown that an isolated domain is deformed substantially from a circular shape when the propagating velocity is increased.

Received January 8, 2012.

Revised February 4, 2013.

2010 *Mathematics Subject Classification.* 37L05, 70K50, 92C10.

Key words and phrases. Excitable reaction-diffusion system, drift bifurcation, interfacial approach, self-propelled motion.

In the present article, we shall describe our recent studies of dynamics of deformable self-propelled domains [3]–[8]. We derive the time-evolution equations for an isolated domain [4], [7] starting with the excitable reaction-diffusion equations [2]. It will be shown that there appears a rich variety of dynamics such as circular motion, zigzag motion, chaotic motion in two dimensions [3], [5] and a helical motion in three dimensions [6], [7]. Dynamics under external fields will also be investigated by numerical simulations and by a kind of phase dynamical approach [8].

In the next section, we introduce the reaction-diffusion equations and derive the time-evolution equations for a single domain. In Section 3, we solve the set of equations numerically in two and three dimensions to obtain various types of self-propelled motion. External forces are added to the time-evolution equations and the dynamics are investigated in two dimensions both numerically and analytically in Section 4. The results are summarized in Section 5.

§2. Time-evolution equations for a domain

We start with a coupled set of reaction-diffusion equations for an activator u and an inhibitor v given by [2]

$$(1) \quad \tau \epsilon \frac{\partial u}{\partial t} = \epsilon^2 \nabla^2 u + f\{u, v\} - v,$$

$$(2) \quad \frac{\partial v}{\partial t} = \nabla^2 v + u - \beta v,$$

where $f\{u, v\} = -u + \vartheta(u - p'\{u, v\})$ with $\vartheta(x) = 1$ for $x > 0$ and $\vartheta(x) = 0$ for $x < 0$. The functional $p'\{u, v\}$ contains a global coupling as

$$(3) \quad p' = p + \sigma \left[\int (u + v) d\vec{r} - W \right],$$

where σ and W are positive constants, $0 < p < 1/2$ and the integral runs over the whole space. The constants τ and β are positive and chosen such that the system is excitable and that a localized stable pulse (domain) solution exists. Inside the domain, the variable u is positive surrounded by the rest state where u and v vanishes asymptotically away from the domain. The parameter ϵ is a measure of the width of the domain boundary (interface). Hereafter we assume that the interface is infinitesimally thin, i.e., $\epsilon \rightarrow 0$. Furthermore, we consider the limit

$\sigma \rightarrow \infty$ so that the global coupling becomes $p' = p$ with

$$(4) \quad \int (u + v) d\vec{r} = W ,$$

and $f\{u, v\}$ is no more a functional but is given by

$$(5) \quad f(u) = -u + \vartheta(u - p) .$$

The constraint (4) means that the area (volume in three dimensions) of a domain is a conserved quantity.

Domain dynamics is uniquely specified if one determines the motion of the interface of domain [4], [7]. Let us put $V(\phi, t)$ as the normal velocity of the interface in two dimensions where ϕ is the angle from the x-axis. The velocity of the center of mass is given by

$$(6) \quad \vec{v} = \frac{1}{A} \int_0^{2\pi} d\phi (R(\phi, t)^2 + (dR(\phi, t)/d\phi)^2)^{1/2} \vec{R}(\phi, t) V(\phi, t) ,$$

where A is the area of the domain, \vec{R} is the position vector at the interface from the center-of-mass position and $R = |\vec{R}|$. Deformations of a domain around a circular shape with radius R_0 are represented in the moving frame at the velocity \vec{v} as

$$(7) \quad R(\phi) = R_0 + \delta R(\phi, t) ,$$

where

$$(8) \quad \delta R(\phi, t) = \sum_{n=-\infty}^{\infty} c_n(t) e^{in\phi} .$$

The modes $n = \pm 1$ related with the translational motion of domain are excluded from the summation. The modes $c_{\pm 2}$ represents an elliptical deformation. We introduce a second rank tensor as follows [4];

$$(9) \quad \begin{aligned} S_{11} &= -S_{22} = c_2 + c_{-2} , \\ S_{12} &= S_{21} = i(c_2 - c_{-2}) . \end{aligned}$$

For an elliptical domain, we may put $c_{\pm 2} = (\delta_2/4) \exp(\mp i 2\phi_2)$ and $R(\phi)$ is represented as

$$(10) \quad R(\phi) = R_0 + \frac{\delta_2}{2} \cos 2(\phi - \phi_2) ,$$

where δ_2 is a positive constant. In this case, the second rank tensor S can be written in terms of the unit vector $\vec{N} = (\cos \phi_2, \sin \phi_2)$ as

$$(11) \quad S_{\alpha\beta} = \delta_2 (N_\alpha N_\beta - \frac{\delta_{\alpha\beta}}{2}).$$

This is equivalent with the nematic order parameter in liquid crystals [11]. The modes $c_{\pm 3}$ are necessary if we consider the head-tail asymmetry of a propagating domain. Let us put $c_{\pm 3} = (\delta_3/2) \exp(\mp i 3\phi_3)$ with a positive constant δ_3 and introduce

$$(12) \quad \vec{N}^{(1)} = (\cos \phi_3, \sin \phi_3),$$

$$(13) \quad \vec{N}^{(2)} = (\cos(\phi_3 + \frac{2\pi}{3}), \sin(\phi_3 + \frac{2\pi}{3})),$$

$$(14) \quad \vec{N}^{(3)} = (\cos(\phi_3 - \frac{2\pi}{3}), \sin(\phi_3 - \frac{2\pi}{3})).$$

The third-rank tensor associated with the $n = \pm 3$ modes is defined in terms of the unit vectors by

$$(15) \quad U_{\alpha\beta\gamma} = \frac{4\delta_3}{3} \sum_{m=1,2,3} N_\alpha^{(m)} N_\beta^{(m)} N_\gamma^{(m)}.$$

From the definitions (12), (13) and (14), we obtain [4]

$$(16) \quad U_{111} = \delta_3 \cos 3\phi_3 = c_3 + c_{-3}$$

$$(17) \quad U_{222} = -\delta_3 \sin 3\phi_3 = -i(c_3 - c_{-3})$$

as well as the relations $U_{111} = -U_{122} = -U_{212} = -U_{221}$ and $U_{222} = -U_{112} = -U_{121} = -U_{211}$. The tensor $U_{\alpha\beta\gamma}$ is the same as the order parameter for banana (tetragonal nematic) liquid crystals in two dimensions [11]. A deformed domain in three dimensions is formulated in terms of the spherical harmonics and the expression of $S_{\alpha\beta}$ is given in Ref. [7].

The time-evolution equations for \vec{v} , $S_{\alpha\beta}$ and $U_{\alpha\beta\gamma}$ can be derived from Eqs. (1) and (2) by means of a singular perturbation for infinitesimally thin interfaces. The assumption is that the propagating velocity is sufficiently small provided that the system is in the vicinity of the supercritical drift bifurcation. The final set of equations is obtained in two dimensions as follows [4].

$$(18) \quad \frac{dv_\alpha}{dt} - \gamma v_\alpha + v_\alpha |\vec{v}|^2 = -a_1 v_\beta S_{\beta\alpha},$$

$$(19) \quad \frac{dS_{\alpha\beta}}{dt} = -\kappa_2 S_{\alpha\beta} + b_1 [v_\alpha v_\beta - \frac{\delta_{\alpha\beta}}{2} \vec{v}^2] + b_2 U_{\alpha\beta\gamma} v_\gamma,$$

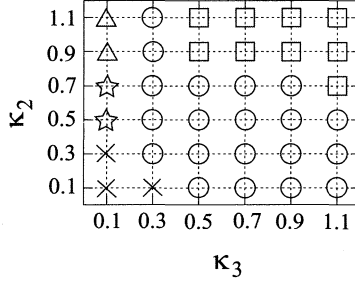


Fig. 1. Phase diagram obtained numerically from Eqs. (18), (19) and (20). Straight motion in the region \square , circular motion in the region \circ , zigzag motion in the region \triangle and chaotic motion in the region of the star symbols. This figure is reproduced from Ref. [5]

$$\begin{aligned}
 \frac{dU_{\alpha\beta\gamma}}{dt} &= -\kappa_3 U_{\alpha\beta\gamma} + d_1 \left[v_\alpha v_\beta v_\gamma - \frac{v_\eta v_\eta}{4} (\delta_{\alpha\beta} v_\gamma + \delta_{\beta\gamma} v_\alpha + \delta_{\gamma\alpha} v_\beta) \right] \\
 &+ \frac{d_2}{3} [S_{\alpha\beta} v_\gamma + S_{\beta\gamma} v_\alpha + S_{\gamma\alpha} v_\beta \\
 (20) \quad &- \frac{v_\eta}{2} (\delta_{\alpha\beta} S_{\gamma\eta} + \delta_{\beta\gamma} S_{\alpha\eta} + \delta_{\gamma\alpha} S_{\beta\eta})],
 \end{aligned}$$

where $\gamma = (\tau_c - \tau)/2$ with τ_c the drift bifurcation threshold. (This γ should not be confused with the one in the suffix of $U_{\alpha\beta\gamma}$.) Even up to the cubic nonlinearity, there are several other terms which, however, are omitted for simplicity. The expressions of the coefficients b_i and d_i are complicated and are referred to the original article [4]. We have derived the time-evolution equations for \vec{v} and $S_{\alpha\beta}$ in three dimensions in Ref. [7].

Before closing this section, we make a remark about the time-evolution equations (18), (19) and (20). Since this represents the motion of the interface of a domain, those are expected to be related with a wave equation in one dimension with a periodic boundary condition. In fact, Armbruster et al have studied mathematically the stability and bifurcation of dissipative nonlinear waves on a closed circle [9, 10]. The set of equations (18), (19) and (20) has some symmetry due to the isotropy of space (see Eqs. (24)–(27) below) whereas the one-dimensional wave equation has a translational invariance. We have identified the various domain motions in two dimensions with the wave solutions in one dimension [5]. In three dimensions, such a correspondence, of course, does not exist.

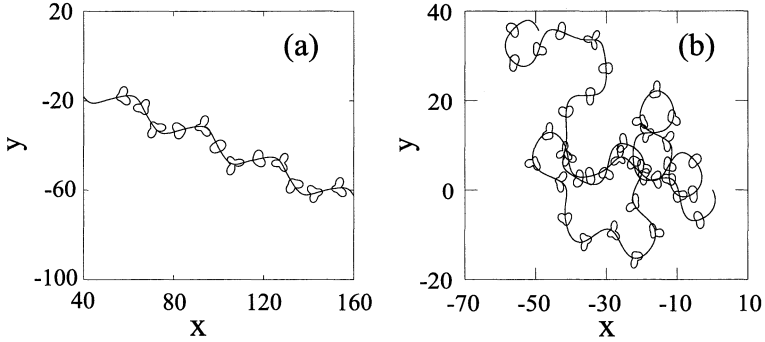


Fig. 2. Snapshots and the trajectory of a zigzag motion (a) and a chaotic motion (b). This figure is reproduced from Ref. [5]

§3. Numerical computation

We have solved numerically Eqs. (18), (19) and (20) for $a_1 = -1.0$, $b_1 = -0.5$, $b_2 = 0.3$, $d_1 = 0.1$, $d_2 = 0.8$ and $\gamma = 1.0$ in two dimensions to obtain the phase diagram displayed in Fig. 1 [5]. When both κ_2 and κ_3 are large, a straight motion appears in the region \square . However, this becomes unstable in the region \circ where a circular motion appears. In the circular motion, the trajectory of a domain exhibits a closed circle. The bifurcation between straight motion and circular motion was predicted in Ref. [3]. Later it was found numerically in a reaction-diffusion system [12]. When the value of κ_3 is small, new motions appear. One is the zigzag motion in the region \triangle as shown in Fig. 2(a) and the other is a chaotic motion in the region of the star symbols as indicated in Fig. 2(b). We have verified numerically that the Lyapunov exponent for this solution is positive. We are unable to identify the motion in the region \times because of numerical instability.

In three dimensions, we have derived a set of equations (18) and (19) without considering the variable $U_{\alpha\beta\gamma}$ [7]. The factor $1/2$ in the second term in Eq. (19) should be replaced by $1/3$. The phase diagram is given in Fig. 3 for $a_1 = -1.0$ and $b_1 = -0.5$ [6]. There are three regions for a rectilinear motion, a circular motion and a helical motion. The solid line is the linear stability threshold of straight motion whereas the broken line is the stability limit of circular motion. The trajectory of a helical motion is displayed in Fig. 4.

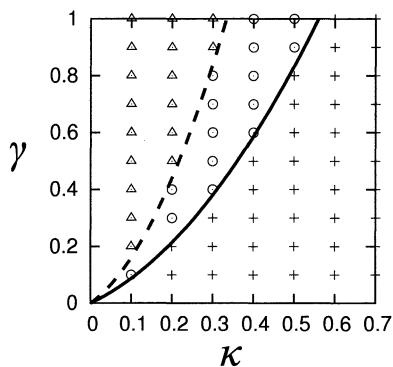


Fig. 3. Phase diagram obtained numerically from Eqs. (18) and (19) in three dimensions. The horizontal axis κ should read κ_2 in Eq. (19). The rectilinear motion is stable in the region indicated by +, circular motion in the region \circ and helical motion in the region Δ . This figure is reproduced from Ref. [6]

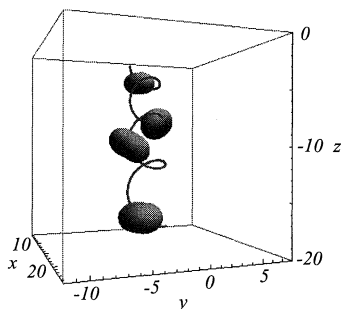


Fig. 4. Trajectory and domain shape of helical motion traveling from top to bottom. This figure is reproduced from Ref. [6]

§4. Motion under external fields

Now we study the motion of a domain under external fields [8]. We consider the simplified set of equations of motion (18) and (19) with

$b_2 = 0$ in two dimensions but adding the external forces

$$(21) \quad \frac{dv_\alpha}{dt} = \gamma v_\alpha - |v|^2 v_\alpha - a S_{\alpha\beta} v_\beta + g_\alpha$$

$$(22) \quad \frac{dS_{\alpha\beta}}{dt} = -\kappa S_{\alpha\beta} + b \left(v_\alpha v_\beta - \frac{1}{2} |v|^2 \delta_{\alpha\beta} \right) + Q_{\alpha\beta},$$

where

$$(23) \quad Q_{\alpha\beta} = h \left(E_\alpha E_\beta - \frac{|E|^2}{2} \delta_{\alpha\beta} \right).$$

The external force g_α is assumed to be given by $\vec{g} = (0, -g)$ with $g > 0$. The other external force E_α in $Q_{\alpha\beta}$ is applied as $\vec{E} = (1, 0)$. Since the tensor $U_{\alpha\beta\gamma}$ is not considered, only straight and circular motions are possible in two dimensions [3] in the absence of the external fields.

Equations (21) and (22) can be written as

$$(24) \quad \frac{dv}{dt} = \gamma v - v^3 - \frac{a}{2} s v \cos 2\psi - g \sin \phi$$

$$(25) \quad \frac{d\phi}{dt} = -\frac{a}{2} s \sin 2\psi - \frac{g}{v} \cos \phi$$

$$(26) \quad \frac{ds}{dt} = -\kappa s + b v^2 \cos 2\psi + h \cos 2\theta$$

$$(27) \quad \frac{d\theta}{dt} = -\frac{b}{2s} v^2 \sin 2\psi - \frac{h}{2s} \sin 2\theta,$$

where we have put $v_1 = v \cos \phi$, $v_2 = v \sin \phi$, $N_1 = \cos \theta$ and $N_2 = \sin \theta$ with v and s positive values, and $\psi = \theta - \phi$. Note that, when the external forces are absent, i.e., $g = h = 0$, only the difference ψ is an independent variable. This comes from the isotropy of space.

First, we show the results of numerical simulations of the model equations (24)–(27) in two dimensions for the gravitational-like external force, i.e., with $g \neq 0$ and $h = 0$. In the numerical computations, the fourth-order Runge–Kutta method is employed with time increment $\delta t = 10^{-4}$. The coupling coefficients a and b are fixed as $a = -1.0$ and $b = -0.5$. The bifurcation threshold between straight motion and circular motion is given by $\gamma_c = 0.18$ for $\kappa = 0.2$. The phase diagram on the γ - g plane is shown in Fig. 5. There are four different motions as shown in Figs. 5(a)–(d): a circular-drift motion, a zigzag-1 motion, a zigzag-2 motion, and a straight-falling motion. In the zigzag-1 motion, the velocity along the y-axis does not change the sign whereas it changes the sign periodically in the zigzag-2 motion. We emphasize two non-trivial dynamics. One is the fact that a straight motion becomes unstable

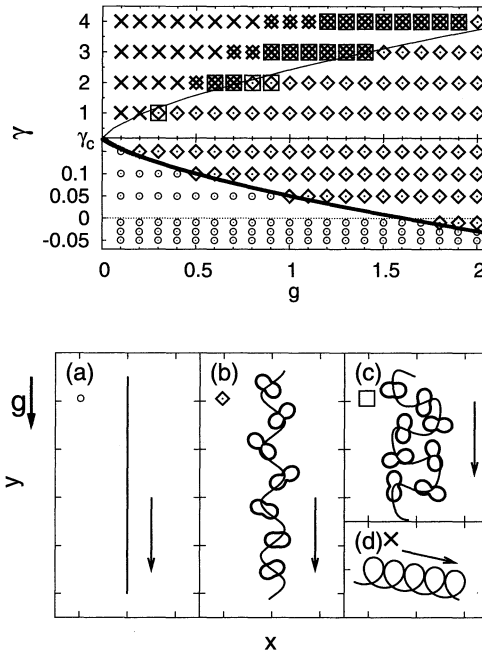


Fig. 5. (Top) Phase diagram on the $\gamma - g$ plane for $\kappa = 0.2$. The symbols indicate the following motions; circular-drift motion (cross), zigzag-1 motion (diamond), zigzag-2 motion (square), and straight-falling motion (circle). Note that there are coexistence regions. (Bottom) Trajectory of (a) the straight-falling motion, (b) zigzag-1 motion, (c) zigzag-2 motion and (d) circular-drift motion. The arrows indicate the direction of migration. The parameters are chosen as $\gamma = 2$ and $\kappa = 0.75$ for (a) and $\gamma = 3$ and $\kappa = 0.2$ for (b), (c) and (d). This figure is reproduced from Ref. [8]

for large values of g even when $\gamma \leq \gamma_c$ in which a straight motion is stable when the external force is absent. The second interesting property is that the domain of a circular-drift motion traverses almost perpendicularly to the direction of the force.

This phase diagram has been analyzed by simplifying eqs. (24)–(27). That is, we eliminate the variables v and s by putting $dv/dt = ds/dt = 0$

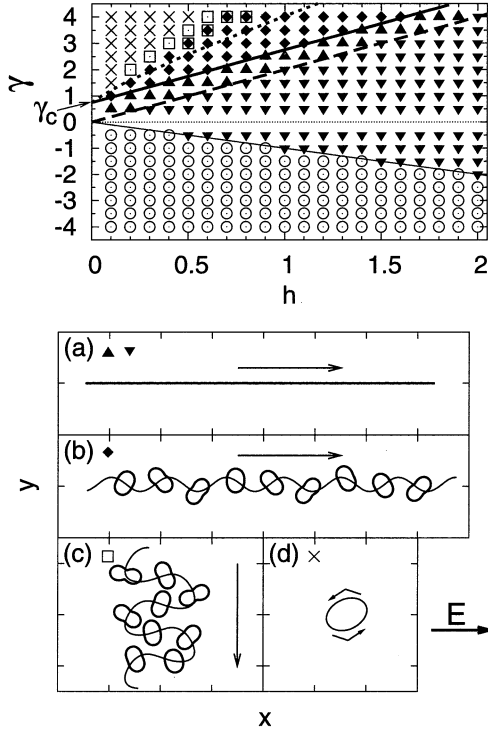


Fig. 6. (Top) Phase diagram on the γ - h plane for $\kappa = 0.5$ obtained numerically from Eqs. (24)–(27). The symbols indicate the circular motion (cross), the zigzag-1 motion (diamond), the zigzag-2 motion (square), and the motionless state (circle). The up (down) triangles indicate the straight motion perpendicular (parallel) to \vec{E} . (Bottom) Trajectories of the center of mass in the real space for $\gamma = 3$ (a) a straight motion for $h = 1.3$, (b) a zigzag-1 motion for $h = 0.6$, (c) a zigzag-2 motion for $h = 0.5$, and (d) a circular motion for $h = 0.3$. This figure is reproduced from Ref. [8]

leaving the set of equations for the angle variables. We may call this method a phase dynamical approach. The lines in Fig. 5 have been obtained from the reduced set of equations. The thin solid line is a

saddle homoclinic-orbit bifurcation boundary whereas the thick solid line is a Hopf bifurcation boundary.

Next, we show the numerical results of self-propulsion in the electric-like external field with $g = 0$ and $h \neq 0$ for $\kappa = 0.5$, $a = -1.0$ and $b = -0.5$. Figure 6 displays, on the γ - h space, the phase diagram of a variety of dynamical states: a circular motion, a zigzag-1 motion, a zigzag-2 motion, and a straight motion. We also show the trajectories of these motions in Figs. 6(a)–(d). When the magnitude of the external force h is large enough, a domain undergoes a straight motion parallel to the electric field for all γ . However, this straight motion is divided into two classes. In the region of the down triangles in Fig. 6, the direction of elongation is parallel to the external force even though we have chosen $b < 0$. In this situation a perpendicular elongation should occur when the external force is absent [3]. The elongation becomes perpendicular for smaller values of h as indicated by the top triangles in Fig. 6. When $\gamma > \gamma_c$, a domain undergoes a circular motion along an elliptically-deformed trajectory as in Fig. 6(d) under a finite but weak external force in the region indicated by the crosses in Fig. 6. Between this circular motion and the straight motion, there is a region indicated by the diamonds where a zigzag-1 motion occurs as displayed in Fig. 6(b). When γ is much larger than $\gamma_c > 0$, there appears another motion, which is called a zigzag-2 motion between the circular motion and the zigzag-1 motion as indicated by the square in Fig. 6. The trajectory is displayed in Fig. 6(c). It should be noted that the migration of the zigzag-2 motion is, on an average, to the direction perpendicular to the external field.

From the reduced set of equations for θ and ϕ , we can determine analytically some of the phase boundaries. The thick solid line in Fig. 6 is a Hopf bifurcation boundary whereas the thin solid line is a pitchfork bifurcation boundary. The thin dotted line is the bifurcation boundary between the circular motion and the zigzag-1 motion obtained numerically from the phase equations.

§5. Summary

We have derived the set of time-evolution equations for a deformable self-propelled domain and have shown that there are circular motion, zigzag motion and helical motion as well as a straight motion by changing the migration velocity and the softness of domain. In three dimensions, a helical motion also appears. By adding the external forces, a gravitational-like force and an electric-like force, the dynamics exhibit much more variety. These dynamical behaviors except for the zigzag-2

motion can be understood by the phase dynamical approach. It is our expectation that the present study gives new insight into the nonlinear domain dynamics far from equilibrium. It is also mentioned the the systems we have studied are closely related with biological systems such as self-propulsion of micro-organisms and living cells.

The author is grateful to T. Ohkuma, T. Hiraiwa, K. Shitara and M. Tarama for their fruitful collaboration in this study. This work was supported by the JSPS Core-to-Core Program “International research network for non-equilibrium dynamics of soft matter” and by Grant-in-Aid for Scientific Research A (No. 24244063) and C (No. 23540449) from JSPS.

References

- [1] L. M. Pismen, *Patterns and Interfaces in Dissipative Dynamics*, Springer, 2006.
- [2] K. Krischer and A. Mikhailov, Bifurcation to traveling spots in reaction-diffusion systems, *Phys. Rev. Lett.*, **73** (1994), 3165–3168.
- [3] T. Ohta and T. Ohkuma, Deformable self-propelled particles, *Phys. Rev. Lett.*, **102** (2009), 154101.
- [4] T. Ohta, T. Ohkuma and K. Shitara, Deformation of a self-propelled domain in an excitable reaction-diffusion system, *Phys. Rev. E*, **80** (2009), 056203.
- [5] T. Hiraiwa, M. Y. Matsuo, T. Ohkuma, T. Ohta and M. Sano, Dynamics of a deformable self-propelled domain, *Europhys. Lett.*, **91** (2010), 20001.
- [6] T. Hiraiwa, K. Shitara and T. Ohta, Dynamics of a deformable self-propelled particle in three dimensions, *Soft Matter*, **7** (2011), 3083–3086.
- [7] K. Shitara, T. Hiraiwa and T. Ohta, Deformable self-propelled domain in an excitable reaction-diffusion system in three dimensions, *Phys. Rev. E*, **83** (2011), 066208.
- [8] M. Tarama and T. Ohta, Dynamics of a deformable self-propelled particle under external forcing, *Eur. Phys. J. B*, **83** (2011), 391–400.
- [9] D. Armbruster, J. Guckenheimer and P. Holmes, Heteroclinic cycles and modulated travelling waves in systems with $O(2)$ symmetry, *Phys. D*, **29** (1988), 257–282.
- [10] D. Armbruster, J. Guckenheimer and P. Holmes, Kuramoto–Sivashinsky dynamics on the center-unstable manifold, *SIAM J. Appl. Math.*, **49** (1989), 676–691.
- [11] L. G. Fel, Tetrahedral symmetry in nematic liquid crystals, *Phys. Rev. E*, **52** (1995), 702–717.
- [12] T. Teramoto, K. Suzuki and Y. Nishiura, Rotational motion of traveling spots in dissipative systems, *Phys. Rev. E*, **80** (2009), 046208.

Department of Physics
Kyoto University, 606-8502
Japan

E-mail address: takao@scphys.kyoto-u.ac.jp